

Multi-Nucleon Transfer Reactions and the Creation and the Evolution of the Compound Nucleus

Matthew Kafker^{1,2} and Aurel Bulgac¹

¹*Department of Physics, University of Washington, Seattle, Washington 98195-1560, USA*

²*Cyclotron Institute, Texas A&M University, College Station, TX 77843 USA*

(Dated: April 24, 2026)

There is no microscopic quantum approach based on the time-dependent Schrödinger equation which has yet to describe the formation of a compound nucleus. The most advanced microscopic approach developed so far to describe multi-nucleon transfer (MNT) reactions in complex nuclear systems is the time-dependent Hartree Fock (TDHF) mean field theory. In any mean field approach, however, the mean field is an expectation value of a quantum operator, and so it is classical in nature and thus its quantum fluctuations are neglected, which are expected to be often crucial. Quantum fluctuations can be in principle be included in a configuration interaction (CI) framework, which in the case of reactions has to be implemented in the continuum. Here we describe the first such implementation within a novel extension of the well known Generator Coordinate Method (GCM), dubbed the enhanced GCM (eGCM), applied to the MNT reaction $^{48}\text{Ca}+^{208}\text{Pb}$ near the Coulomb barrier, which demonstrates significant qualitative differences with either TDHF or GCM previous approaches. It appears that eGCM is the first theoretical approach capable of predicting the compound nucleus formation cross section, thus a nuclear molasses, the counterpart to optical molasses.

Ninety years ago Niels Bohr introduced based on qualitative arguments the concept of a compound nucleus [1, 2], which has been widely used in nuclear physics ever since. No microscopic derivation based on the many-body Schrödinger equation was ever convincingly demonstrated however and, thus using mathematical terminology, the compound nucleus is simply a theoretical conjecture, amply used however in phenomenological approaches. In the editorial to the Bohr [1] paper, the compound state is pictorially described as a superposition of a very large number of “simpler” many-body states, which basically form a continuum and the best guess anybody has currently is that the coefficients in this expansion are complex random numbers, according to the Wigner-Dyson surmise in Random Matrix Theory [3], which has been studied in the case of the nuclear shell-model [4, 5] in particular, and the relation between classical and quantum chaos in quantum systems with a relatively small number of degrees of freedom [6–9], but never for nuclear reactions between heavy-ion nuclei or fission, processes which are strongly non-equilibrium time-dependent phenomena. The multi-nucleon transfer reactions are in a somewhat better position, as an incomplete theoretical framework exists, the Time-Dependent Hartree-Fock (TDHF) method.

MNT reactions are the tool of choice to produce new nuclides. One of the most fundamental questions in physics is how many elements exists, or more precisely, how any isotopes exist on Earth or can be created, and what is the mechanism of their creation, in the laboratory and in Nature in the collisions of neutron stars and black holes and in supernova collapses [10–12]. Elements from $Z = 1$ (Hydrogen) to $Z = 92$ (Uranium) were all discovered on Earth until 1939, except Technetium. Concerning the question about how many isotopes exist naturally on Earth, the answer is about 339, including 251 sta-

ble isotopes. Among the rest of the predicted 7000-8000 possible isotopes [13, 14], only about 3,000-3,300 have been created so far in many laboratories throughout the World [15]. While most of these predicted isotopes are not naturally stable, their even rather short-time existence as an intermediate stage in the creation of other elements and isotopes is crucial in order to predict the abundances in the Solar system in particular. The overwhelming number of nuclei and isotopes not found naturally on Earth have been created in multi-nucleon transfer (MNT) heavy-ion reactions and the quest to identify the rest of them is an ongoing process. Unfortunately, there’s still no microscopic framework accurate enough to replace the many existing phenomenological models, which are based on various assumptions, many fitting parameters, and are overwhelmingly classical in their character. These approaches have been discussed in the recent overview and in Refs. [16–23], in which cases the typical phenomenological equation used is [16, 17]

$$\sigma_{EVR} = \sum_{J=0}^{J_{\max}} \sigma_{\text{cap}}(E_{\text{CoM}}, J) P_{\text{CN}}(E^*, J) W_{\text{sur}}(E^*, J), \quad (1)$$

where the compound nucleus formation probability P_{CN} is always purely phenomenological with wide variations.

The most sophisticated microscopic model existing in the literature is the time-dependent mean field theory in either its TDHF incarnation or in its extension, the time-dependent Density Functional Theory (TDDFT), an approach which is based on the adequacy of using mean field which is classical in character, see one of the most recent papers [21], where many references to various methods suggested so far in literature over many decades are given. This deficiency of the mean field approximation can be removed in a configuration interaction (CI) framework, of which the generator coordinate method (GCM) was

believed for a long time to be a good solution [24–27], although this claim was recently challenged with the introduction of the enhanced GCM (eGCM) framework [28].

The GCM [25] is basically a CI-method based on linearly independent non-orthogonal system of ground state static Slater determinants with fixed shapes, which were assumed to describe an adiabatically evolving nucleus from the neutron capture to scission in induced fission [25, 29, 30]. In the case of heavy-ion reactions however the reaction fragments acquire significant excitation energy, not accounted for in an adiabatic evolution as Reinhard *et al.* [26] noticed, which also happens in induced fission [31–34]. The corresponding many-body wave functions for the three approaches are defined as

$$\Psi_{\text{GCM}}(\xi_1 \dots \xi_A) = \int_Q f(Q) \Phi(\xi_1 \dots \xi_A | Q), \quad (2)$$

$$\Psi_{\text{GCM}_R}(\xi_1 \dots \xi_A, t) = \int_Q f(Q, t) \Phi(\xi_1 \dots \xi_A | Q, t), \quad (3)$$

$$\Psi_{\text{eGCM}}(\xi_1 \dots \xi_A) = \int_{Q, \tau} f(Q, \tau) \Phi(\xi_1 \dots \xi_A | Q, \tau). \quad (4)$$

The difference between Ψ_{GCM} and Ψ_{GCM_R} is the time dependence of the Slater determinants in the latter [26]. eGCM [28] on the other hand is a “bouillabaisse” of linearly independent non-orthogonal time-dependent Slater determinants generated with a large set of initial conditions and all mixed at many times along their TDDFT trajectories, and thus basically a path integral along the TDHF trajectories.

We will demonstrate here that the enhanced GCM (eGCM) is indeed a many-body framework, which leads to a many-body wave functions of extreme complexity describing the collision of heavy ions in particular, which has the expected symmetry from quantum mechanics. We demonstrate that a very large number of relevant many-body configurations were ignored in all previous incarnations of GCM. This is an argument in line with what one would expect from the Fermi golden rule, namely that the number of relevant final states is controlled not only by the magnitude of average transition matrix element, but more importantly, by the number of such accessible final states.

In any scattering of a plane wave of an unpolarized projectile on an unpolarized target the many-body wave function has an azimuthal symmetry around the axis of the impinging beam, which is faithfully reproduced in eGCM as described here. The components of this plane wave corresponding to relatively large impact parameters interact with the target only due to the role of the long range Coulomb repulsion between the reaction partners and nucleon transfer is suppressed. Only those impact parameters where the two reaction fragments come into the range of the nucleon-nucleon interaction might significantly contribute to nucleon transfer. One has to distinguish at this point between glancing collisions and collisions at small impact parameters of the two reaction fragments, the latter of which can lead to very long lived “compound-like states” [1], and these will not be incor-

porated at this stage into the eGCM framework. For collision energies below the Coulomb barrier, the nucleon transfer is expected to have an essentially tunneling under the barrier character and thus be significantly suppressed. Simenel *et al.* [22] discuss in their recent work the role of the contact time in $^{40\dots 56}\text{Ca} + ^{176}\text{Yb}$ collisions at energies just above the Coulomb barrier and demonstrate that the formation of reaction fragments heavier than the target (which is usually the heavier nucleus) occurs only for relatively short contact times between the reaction fragments. These are the kind of reactions we will discuss in this initial implementation of eGCM to nuclear reactions. We will describe the collision $^{48}\text{Ca} + ^{208}\text{Pb}$ at a center-of-mass energy 235 MeV, which is slightly above the Coulomb barrier between the two initial partners, in both a time-independent and a time-dependent frameworks, as these points of view have different physical interpretations. This reaction has been studied experimentally and theoretically [35, 36], where the phenomenon of quasi-fission is dominant. At long contact times the $^{256}_{102}\text{No}_{154}$ non-equilibrated nucleus is formed during central collisions of the two initial reaction fragments, experiencing both quasi-fission and fission stages. One can thus separate to a rather good approximation the time evolution of such a collision roughly into a fast and a slow phase, characterized by the contact time between the two reaction partners.

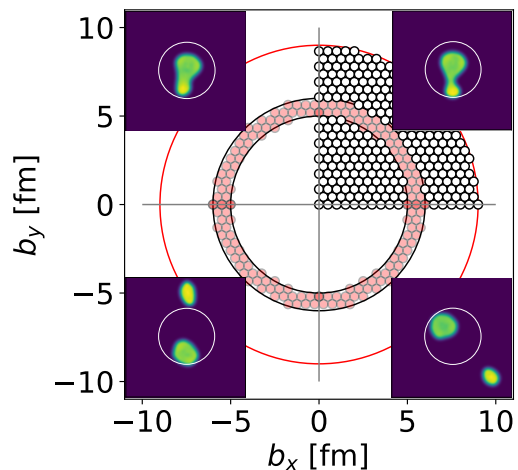


FIG. 1. In the impact parameter plane $\mathbf{b} = (b_x, b_y)$ only the impact parameter points with centers inside the red ring, with $|\mathbf{b}| \approx 5-6$ fm, were considered. The insets show representative density profiles from the TDHF simulations. On the left are trajectories with $\mathbf{b} = (5, 0)$ and on the right with $\mathbf{b} = (6, 0)$. In the upper frames $t = 420$ fm/c and the lower frames are shown at their final time. The white circles in the insets indicate the region in which particle number projection is performed at late times.

As a first step we perform TDDFT simulations (with no pairing) of the collision $^{48}\text{Ca} + ^{208}\text{Pb}$ at energies

slightly above the Coulomb barrier with the impact parameters within a ring in the impact parameter space shown in Fig. 1 and we stored the TDDFT single-particle wave functions $\phi_k(\alpha)$, where $k = 1, \dots, 256$ and $\alpha = (b_x, b_y, \tau)$, at various times τ along each TDDFT trajectory labelled by the impact parameter \mathbf{b} . The TDDFT simulations are performed with the energy density functional SeaLL1 [14] in a simulation box 64^3 with a lattice constant 1 fm and with the code LISE [37]. The storage of the TDDFT single-particle wave functions used in our study required about 80 TB of memory, and the construction of the eGCM Hamiltonian matrix was performed using 48,000 GPUs on the Frontier supercomputer at Oak Ridge National Lab. The number of times τ the TDDFT wave functions stored for use in GCM calculation was $N_\tau = 385$ with a step $\Delta\tau = 6.4$ fm/c. The total number of impact parameters in the red ring in Fig. 1 was $N_{\mathbf{b}} = 152$ and the size of the GCM matrix was 39,630, which is arguably one of the largest basis sets ever used in a nuclear GCM calculation, and particularly in the continuum. For particle number projection in the final state, we used 56,000 GPUs.

The next step is to introduce the eigenvalues and eigenvectors of the norm overlap matrix between various Slater determinants, and to introduce two new set orthogonal linear combinations of Slater determinants $|\bar{\Phi}_k\rangle$ and $|\bar{\Phi}(\alpha)\rangle$, which are used for the formulation of the static eGCM equation, Eqs. (8),

$$\int_{\alpha'} \langle \Phi(\alpha) | \Phi(\alpha') \rangle g_k(\alpha') = \nu_k g_k(\alpha), \quad \nu_k \geq 0, \quad (5)$$

$$\int_{\alpha} g_k^*(\alpha) g_l(\alpha) = \delta_{kl}, \quad \int_{\alpha} g_k(\alpha) g_k^*(\beta) = \delta(\alpha - \beta), \quad (6)$$

$$|\bar{\Phi}_k\rangle = \int_{\alpha} \nu_k^{-1/2} g_k(\alpha) |\Phi(\alpha)\rangle, \quad \nu_k > 0, \quad \langle \bar{\Phi}_n | \bar{\Phi}_m \rangle = \delta_{nm} \quad (7)$$

$$\langle \bar{\Phi}_k | \hat{H} | \Psi_n \rangle = \int_{\alpha} \langle \bar{\Phi}_k | \hat{H} | \bar{\Phi}_l \rangle h_{ln} = h_{kn} E_n, \quad (8)$$

$$|\bar{\Phi}(\alpha)\rangle = \int_{\alpha'} g_l^*(\alpha) |\bar{\Phi}_l\rangle, \quad \langle \bar{\Phi}(\alpha) | \bar{\Phi}(\beta) \rangle = \delta_{\alpha\beta}, \quad (9)$$

$$\langle \bar{\Phi}(\alpha) | \hat{H} | \Psi_n \rangle = \int_{\beta} \langle \bar{\Phi}(\alpha) | \hat{H} | \bar{\Phi}(\beta) \rangle h_{\beta n} = h_{\alpha n} E_n, \quad (10)$$

where $\alpha = (\mathbf{b}, \tau)$, with τ being the additional, crucial generator coordinate that distinguishes eGCM from all previous GCM-type approaches in the literature. The eGCM formulations in Eqs. (8, 10) are each equivalent to a CI solution of the many-body problem in the continuum in the present case. The relation between the many-body wave functions sets $|\bar{\Phi}_k\rangle$ and $|\bar{\Phi}(\alpha)\rangle$ is similar to the relation between the Bloch and Wannier wave functions in crystals [38] and a similar relation between localized (sinc(x)) and delocalized wave functions in the discrete variable representation method (DVR) [39].

A very useful measure of the complexity of the eGCM many-body wave functions, which reflects the degree of mixing between different TDDFT trajectories, are the inverse participation ratios (IPR) for the norm and Hamil-

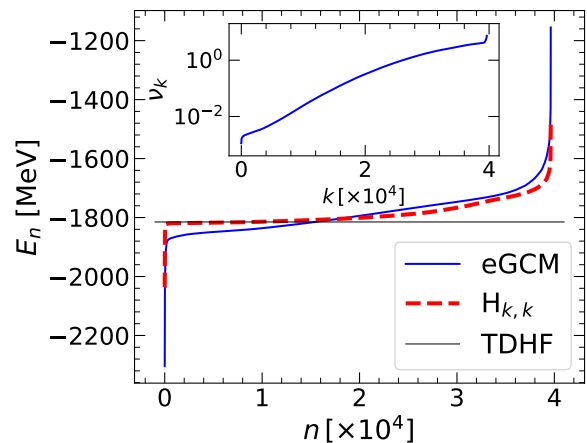


FIG. 2. The eGCM energies (blue line) for all trajectories used in this analysis versus the diagonal matrix elements $\langle \bar{\Phi}_k | \hat{H} | \bar{\Phi}_k \rangle$ (red dashed line). The inset displays the eigenvalues ν_k of the corresponding norm overlaps (NB $\nu_k \neq 0$).

tonian overlaps

$$\text{IPR}_N(k) = \left[\int_{\alpha} |g_k(\alpha)|^4 \right]^{-1}, \quad \text{IPR}_N(\alpha) = \left[\int_{k} |g_k(\alpha)|^4 \right]^{-1},$$

$$\text{IPR}_H(n) = \left[\int_{k} |h_{k,n}|^4 \right]^{-1}, \quad \text{IPR}_H(\alpha) = \left[\int_{k} |h_{\alpha,n}|^4 \right]^{-1}.$$

Our calculations show that the norm and Hamiltonian overlaps are not ever close in shape to a Gaussian and the Gaussian overlap approximation cannot be used in eGCM [40]. Related issues concerning the agreement between exact TDGCM and TDGCM+GOA have been discussed in the literature, which show significant discrepancies between the two approaches [41].

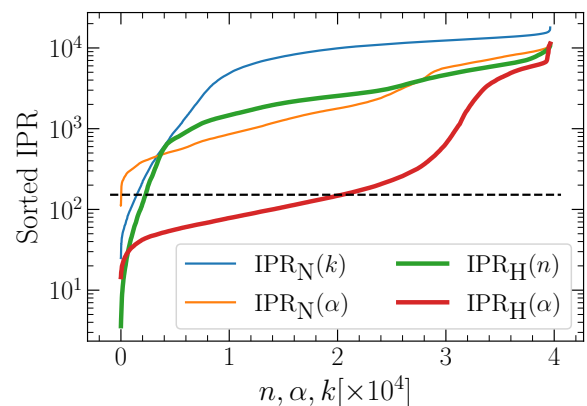


FIG. 3. The IPR for the Norm (thin lines) and the Hamiltonian (thick lines) eGCM overlaps. The maximum possible IPR for the GCM_R overlaps is shown with a dashed line.

If the eigenvectors and the eigenvalues of Eq. (8) are determined one can easily construct the solution of the time-dependent eGCM (TDeGCM) equation with speci-

fied initial conditions

$$i\hbar\partial_t|\Psi(t)\rangle = \hat{H}|\Psi(t)\rangle, \quad \langle\Psi(t)|\Psi(t)\rangle = 1, \quad (11)$$

$$|\Psi(t)\rangle = \sum_n c_n(t)|\Psi_n\rangle, \quad c_n(t) = c_n(0) \exp\left(-\frac{iE_n t}{\hbar}\right), \quad (12)$$

$$c_n(0) = \langle\Psi_n|\Psi(0)\rangle = \mathcal{N} \sum_{\mathbf{b}} \sum_k g_k^*(\mathbf{b}, 0) \nu_k^{1/2} h_{kn}^*, \quad (13)$$

and \mathcal{N} is the normalization. The initial many-body wave function is a uniform superposition over all initial states in the ring of impact parameters illustrated in Fig. 1, and so the many-body wave function has by construction the expected azimuthal symmetry. In the TDeGCM with initial conditions as we described above the total energy $E_{tot} = \langle\Psi(t)|\hat{H}|\Psi(t)\rangle$ is conserved. Since $|\Psi(t)\rangle$ is a superposition of eigenstates the initial state has a mean energy $E_{tot} = -1817.5$ MeV and a standard deviation $\Delta E = 27.9$ MeV. Since $\Delta E \Delta \tau < \hbar$ and initial relative velocity of the two nuclei $v_{rel} = 0.113c$ is significantly smaller than the Fermi velocity, the discretization $\Delta \tau$ and $\Delta \mathbf{b}$ (see Fig. 1) appear to be quite satisfactory. Eq. (12) demonstrates that once there is a full solution of any static GCM implementation, there is no need for a GCM time-dependent code [42–45]. One can introduce then the IPR for the time-dependent many-body wave function $|\Psi(t)\rangle$

$$|\Psi(t)\rangle = \sum_k a_k(t)|\bar{\Phi}_k\rangle = \sum_{\alpha} d(\alpha|t)|\bar{\Phi}(\alpha)\rangle, \quad (14)$$

using the either $a_k(t)$ or $d(\alpha|t)$ expansion coefficients. The probabilities to find N and Z neutrons and protons in the heavy reaction fragment is given by [46, 47]

$$P_H(N, Z) = \iint \frac{d\eta_N d\eta_Z}{(2\pi)^2} \langle\Psi(t)|e^{i\eta_N(\hat{N}_N - N)} e^{i\eta_Z(\hat{N}_Z - Z)}|\Psi(t)\rangle,$$

$$\hat{N}_{N,Z} = \sum_{\mathbf{r}, \sigma} \Theta_H(\mathbf{r}) \psi^\dagger(\xi) \psi(\xi),$$

where $\hat{N}_{N,Z}$ is the neutron/proton number operator, ξ stand for space-spin-isospin coordinates, $|\Psi(t)\rangle$ is the final many-body wave function and $\Theta_H(\mathbf{r})$ is non-vanishing in the heavy reaction fragment region.

In the case of the extension of GCM due to Reinhard *et al.* [26], denoted here GCM_R, both the norm overlap and the Hamiltonian overlap matrices have a block-diagonal structure with $\langle\Phi(\mathbf{b}, \tau)|\Phi(\mathbf{b}', \tau')\rangle \propto \delta_{\tau, \tau'}$ and $\langle\Phi(\mathbf{b}, \tau)|\hat{H}|\Phi(\mathbf{b}', \tau')\rangle \propto \delta_{\tau, \tau'}$, where the number of impact parameters in the present case is typically $< N_b = 152$, unlike in the case of eGCM where the dimension of the corresponding matrices is 39,630 in our simulations (arguably the largest GCM simulation ever reported in the literature) [28]. The kinetic energies of all the included TDDFT trajectories are 235 MeV, and the total TDHF energy is shown with the thin solid line in Fig. 2. The spectrum in Fig. 2 shows an enormous degree of almost degeneracy around the TDDFT energy. Within eGCM the basis set is constructed from $N_b = 152$ full TDHF trajectories, with impact parameters between 5

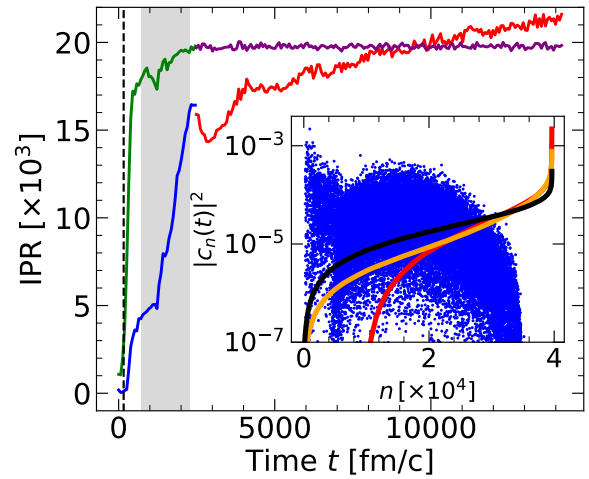


FIG. 4. The IPR is evaluated for the wave function $|\Psi(t)\rangle$, see Eq. (14), using either the expansion coefficients $a_k(t)$ (blue line, continued red after $t_{fin} = 2,482$ fm/c), and coefficients $d(\alpha|t)$ (green line, continued purple after t_{fin}). The vertical black dashed line indicates the time when all the nuclei first make contact in TDHF. The gray banded region indicates the range of times during which the nuclei separate in TDHF. The inset displays the coefficients $|c_n(t)|^2$, as well as the sorted coefficients $|d(\alpha|t_{fin})|^2$, $|a_k(t_{fin})|^2 \times 1.75$, and $|c_n(t_{fin})|^2$ with black, orange, and red lines respectively.

and 6 fm, in all of which the reaction fragments separate at the end of the simulation.

The inverse participation ratios (IPR) for the norm and energy overlaps provide more insights into the structure and the physical interpretations of the eGCM versus the GCM_R wave functions. Fig. 3 alone demonstrates the overwhelming superiority of the eGCM over GCM_R. In case of nuclear pairing correlations for example the spreading of nucleon pairs over about ten degenerate orbitals leads to the what many would call a “phase transition” in a finite system, as seen for example in the magic ^{100}Sn versus the neutron superfluid ^{120}Sn . The eGCM Hamiltonian and norm overlaps IPRs are more than two orders of magnitude larger than the maximum value in the case of GCM_R, which is $N_b = 152$ and which was hoped for more than four decades now to lead to a satisfactory description of nuclear reactions [20, 26, 48–53].

Once the incident projectile and target come into contact, the IPR starts rising dramatically, see Fig. 4. Reaction fragments originating from different impact parameters \mathbf{b} and \mathbf{b}' arrive or leave this interaction region at slightly different times τ and τ' and that leads to mixing between trajectories after the reaction fragments separate, in the gray region in the Fig. 4.

Perhaps the most unexpected result emerging from eGCM treatment of MNT reactions is the stark difference with the results of TDHF simulations. In all our TDHF simulations, the two nuclei came into contact in about $t_c = 162$ fm/c and all of them separated well before we stopped our simulations at $t_f = 2,482$ fm/c. The trajec-

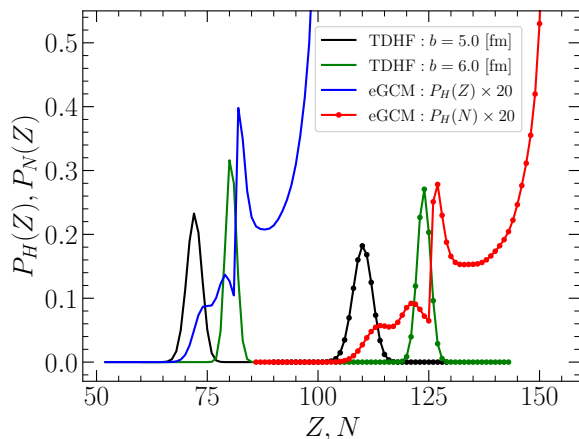


FIG. 5. Final probabilities $P_H(N) = \sum_Z P_H(N, Z)$ (red lines) and $P_H(Z) = \sum_N P_H(N, Z)$ (blue lines) showcasing the dramatic differences between TDHF and eGCM. The solid dotted black and green lines are the TDHF probabilities $P_H(N)$ or $P_H(Z)$ for the heavy fragments and solid without dots for $P_L(N)$ or $P_L(Z)$.

tories with $b = 5$ fm separate at $t_s = 2,262$ fm/c and those with $b = 6$ fm separate at $t_s = 775$ fm/c, meaning that the nucleus spends 85% and 25% of the total simulation time in the transitional “compound system configuration” for $b = 5$ fm and $b = 6$ fm respectively. In eGCM however we observed the formation of a “compound nucleus,” $^{256}_{102}\text{No}_{154}$, with an excitation energy $E_{ex} \approx 78$ MeV, with $Z = 102$ protons and $N = 154$ neutrons with a probability $P_H(154, 102) = 0.34$, which is totally unexpected, a result never found in any previous TDHF MNT simulations, see Fig. 5. We find furthermore that this compound nucleus is an extremely long-lasting state, and does not break apart even when simulated for very long times, a result totally at odds with all TDHF trajectories included in our basis. We also find that $\sum_{N=1}^{126} \sum_{Z=83}^{102} P_H(N, Z) \approx 0.012$ and $\sum_{N=127}^{154} \sum_{Z=1}^{82} P_H(N, Z) \approx 0.006$, indicated that MNT favors transfer in either directions of both protons and neutrons. The most surprising outcome however is that $\sum_{N=127}^{154} \sum_{Z=83}^{102} P_H(N, Z) \approx 0.85$ by far the dominant probability, while $\sum_{N=1}^{126} \sum_{Z=1}^{82} P_H(N, Z) \approx 0.13$.

We used the eGCM energy spectrum, see Eqs. (8,10), to establish if the properties of our “compound nucleus” are consistent with the Wigner-Dyson surmise in Random Matrix Theory [3–5], and thus in agreement with

Bohr [1] compound hypothesis. Our eGCM spectrum has a quite low average level spacing ≈ 4 keV, and the normalized distribution of level spacings in eGCM has a standard deviation of 0.5273, in close agreement with the value 0.5227 which one obtains in the Gaussian Orthogonal Ensemble (GOE). This proves that eGCM is capable of describing a “compound nucleus.” The proton and neutron numbers, average and standard deviation, for the heavy fragment are 97.6 ± 7.3 and 147.4 ± 10.2 , which demonstrates that even in glancing collisions a significant number of neutrons and protons are transferred predominantly to the heavy target, in contrast to TDHF.

Unfortunately, the analysis of the available experimental results [35, 36], is beyond the scope of this first implementation of eGCM and requires the theoretical study of the fission and quasi-fission of the “created compound nucleus” which we described here, which even though it is feasible using theoretical tools recently developed in TDDFT, also requires their extension to eGCM, see Ref. [28] and many references therein.

In summary, eGCM is clearly superior to the tools used so far in the literature and it also points to a degree of quantum interference among the components of the eGCM many-body wave functions never encountered so far in nuclear physics, at least in any analysis we are aware of. This destructive interference, manifested in high probability to form a “compound nucleus” with very high Z and very high N , $P(^{256}_{102}\text{No}_{154}) = 0.34$, is the quantum explanation of why the created “compound nucleus” has an enormous life-time. In eGCM the role of nucleon-nucleon collisions, in particular neutron-proton collisions is significantly enhanced.

We thank I. Stetcu, I. Abdurrahman and G. A. Miller for discussions. AB acknowledges the funding from the Department of Energy Office of Science, Grant No. DE-FG02-97ER41014. This material is additionally based upon work supported by the Department of Energy, National Nuclear Security Administration, under Award Number DE-NA0004150, the Center for Excellence in Nuclear Training And University-based Research (CENTAUR). This research used resources of the Oak Ridge Leadership Computing Facility, which is a U.S. DOE Office of Science User Facility supported under Contract No. DE-AC05-00OR22725.

[1] N. Bohr, “Neutron Capture and Nuclear Constitution,” *Nature* **137**, 344 (1936).
[2] Editorial, “Neutron Capture and Nuclear Constitution,” *Nature* **137**, 351 (1936).
[3] M. L. Mehta, *RANDOM MATRICES and the Statistical Theory of Energy Levels* (Academic Press, New York, 1991).
[4] M. Horoi, V. Zelevinsky, and B. A. Brown, “Chaos vs

Thermalization in the Nuclear Shell Model,” *Phys. Rev. Lett.* **74**, 5194 (1995).
[5] V. Zelevinsky, B. A. Brown, N. F., and M. Horoi, “The nuclear shell model as a testing ground for many-body quantum chaos,” *Phys. Rep.* **276**, 85 (1996).
[6] O. Bohigas, M. J. Giannoni, and C. Schmit, “Characterization of Chaotic Quantum Spectra and Universality of Level Fluctuation Laws,” *Phys. Rev. Lett.* **52**, 1 (1984).

- [7] O. Bohigas, S. Tomsovic, and D. Ullmo, “Manifestations of classical phase space structures in quantum mechanics,” *Physics Reports* **223**, 43–133 (1993).
- [8] M. V. Berry, “Les Houches LII, Chaos and Quantum Physics,” (North-Holland, Amsterdam, 1991).
- [9] F. Haake, S. Gnutzmann, and M. Kuš, *Quantum Signatures of Chaos* (Springer, 2018).
- [10] M. Thoennessen, “Reaching the limits of nuclear stability,” *Rep. Prog. Phys.* **67**, 1187 (2004).
- [11] M. Thoennessen, “Discovery of Nuclides Project: Brief History of Rare Isotopes,” (2024).
- [12] M. Thoennessen, *The Discovery of Isotopes* (Springer, 2015).
- [13] J. Erler, N. Birge, M. Kortelainen, and *others*, “The limits of the nuclear landscape,” *Nature* **486**, 509 (2012).
- [14] A. Bulgac, M. M. Forbes, S. Jin, R. Navarro Perez, and N. Schunck, “Minimal nuclear energy density functional,” *Phys. Rev. C* **97**, 044313 (2018).
- [15] “Ranking of Laboratories,” .
- [16] W Loveland, “Synthetic Paths to the Heaviest Elements,” *J. Phys.: Conf. Ser.* **420**, 012004 (2013).
- [17] K. Godbey and *others*, “Paths to Superheavy Nuclei,” *J. Phys. G: Nucl. Part. Phys.* **52**, 120501 (2025).
- [18] D. D. Zhang, D. Vretenar, T. Nikšić, P. W. Zhao, and J. Meng, “Multinucleon transfer with time-dependent covariant density functional theory,” *Phys. Rev. C* **109**, 024614 (2024).
- [19] B. Li, D. Vretenar, T. Nikšić, D. D. Zhang, P. W. Zhao, and J. Meng, “Entanglement in multinucleon transfer reactions,” *Phys. Rev. C* **110**, 034611 (2024).
- [20] B. Li, D. Vretenar, T. Nikšić, P. W. Zhao, and J. Meng, “Microscopic model for yields and total kinetic energy in nuclear fission,” *Phys. Rev. C* **111**, L051302 (2025).
- [21] Z. Wu, X.-X. Sun, and L. Guo, “Impact of octupole correlation on the inverse quasifission in $^{160}\text{Gd} + ^{186}\text{W}$ collisions,” *Phys. Rev. C* **113**, 024618 (2026).
- [22] C. Simenel, A.S. Umar, K. Godbey, and P. McGlynn, “Shell effects in quasi-fission for calcium induced reactions forming thorium isotopes,” *Phys. Lett. B* **871**, 139955 (2025).
- [23] O. Fasoula and *others*, “Peripheral heavy-ion collisions below the Fermi energy: The case of $^{86}\text{Kr} + ^{64}\text{Ni}$ and $^{86}\text{Kr} + ^{124}\text{Sn}$ at 15 MeV/nucleon,” *Phys. Rev. C* **113**, 034621 (2026).
- [24] R. E. Peierls and J. Yoccoz, “The collective model of nuclear motion,” *Proc. Phys. Soc. A* **70**, 381 (1957).
- [25] J. J. Griffin and J. A. Wheeler, “Collective Motions in Nuclei by the Method of Generator Coordinates,” *Phys. Rev.* **108**, 311 (1957).
- [26] P.-G. Reinhard, R.Y. Cusson, and K. Goeke, “Time evolution of coherent ground-state correlations and the TDHF approach,” *Nucl. Phys. A* **398**, 141 (1983).
- [27] P. J. Reinhard and K. Goeke, “The generator coordinate method and quantised collective motion in nuclear systems,” *Rep. Prog. Phys.* **50**, 1 (1987).
- [28] A. Bulgac, “A critical assessment of the current implementations of the Generator Coordinate Method, accepted to be published in *Phys. Rev. C*,” (2024), [arXiv:2408.02173 \[nucl-th\]](https://arxiv.org/abs/2408.02173).
- [29] N. Bohr and J. A. Wheeler, “The Mechanism of Nuclear Fission,” *Phys. Rev.* **56**, 426 (1939).
- [30] D. L. Hill and J. A. Wheeler, “Nuclear Constitution and the Interpretation of Fission Phenomena,” *Phys. Rev.* **89**, 1102 (1953).
- [31] A. Bulgac, P. Magierski, K. J. Roche, and I. Stetcu, “Induced Fission of ^{240}Pu within a Real-Time Microscopic Framework,” *Phys. Rev. Lett.* **116**, 122504 (2016).
- [32] A. Bulgac, S. Jin, K. J. Roche, N. Schunck, and I. Stetcu, “Fission dynamics of ^{240}Pu from saddle to scission and beyond,” *Phys. Rev. C* **100**, 034615 (2019).
- [33] A. Bulgac, S. Jin, and I. Stetcu, “Nuclear Fission Dynamics: Past, Present, Needs, and Future,” *Frontiers in Physics* **8**, 63 (2020).
- [34] M. Bender and *et al.*, “Future of nuclear fission theory,” *J. Phys. G: Nucl. Part. Phys.* **47**, 113002 (2020).
- [35] E.V. Prokhorova and *others*, “The fusion–fission and quasi-fission processes in the reaction $48\text{Ca} + 208\text{Pb}$ at energies near the Coulomb barrier,” *Nucl. Phys. A* **802**, 45 (2008).
- [36] D.J. Hinde, M. Dasgupta, and E.C. Simpson, “Experimental studies of the competition between fusion and quasifission in the formation of heavy and superheavy nuclei,” *Prog. Part. Nucl. Phys.* **118**, 103856 (2021).
- [37] S. Jin, K. J. Roche, I. Stetcu, I. Abdurrahman, and A. Bulgac, “The LISE package: solvers for static and time-dependent superfluid local density approximation equations in three dimensions,” *Comp. Phys. Comm.* **269**, 108130 (2022).
- [38] N. W. Ascroft and N. D. Mermin, *Solid State Physics* (Saunders College, 1976).
- [39] A. Bulgac and M. M. Forbes, “Use of the discrete variable representation basis in nuclear physics,” *Phys. Rev. C* **87**, 051301(R) (2013).
- [40] M. Kafker, “New Developments in Fermionic Many-Body Physics within Time-Dependent Density Functional Theory,” (2025).
- [41] M. Verrière, N. Dubray, N. Schunck, D. Regnier, and P. Dossantos-Uzarralde, “Fission description: First steps towards a full resolution of the time-dependent Hill-Wheeler equation,” *EPJ Web Conf.* **146**, 04034 (2017).
- [42] D. Regnier, N. Dubray, M. Verrière, and N. Schunck, “FELIX-2.0: New version of the finite element solver for the time dependent generator coordinate method with the Gaussian overlap approximation,” *Comp. Phys. Com.* **225**, 180 (2018).
- [43] D. Regnier, N. Dubray, N. Schunck, and M. Verrière, “Fission fragment charge and mass distributions in $^{239}\text{Pu}(n, f)$ in the adiabatic nuclear energy density functional theory,” *Phys. Rev. C* **93**, 054611 (2016).
- [44] M. Verriere and D. Regnier, “The Time-Dependent Generator Coordinate Method in Nuclear Physics,” *Front. Phys.* **8**, 233 (2020).
- [45] M. Verriere, N. Schunck, and D. Regnier, “Microscopic calculation of fission product yields with particle-number projection,” *Phys. Rev. C* **103**, 054602 (2021).
- [46] C. Simenel, “Particle Transfer Reactions with the Time-Dependent Hartree-Fock Theory Using a Particle Number Projection Technique,” *Phys. Rev. Lett.* **105**, 192701 (2010).
- [47] A. Bulgac, “Projection of good quantum numbers for reaction fragments,” *Phys. Rev. C* **100**, 034612 (2019).
- [48] D. Regnier and D. Lacroix, “Microscopic description of pair transfer between two superfluid Fermi systems. II. Quantum mixing of time-dependent Hartree-Fock-Bogolyubov trajectories,” *Phys. Rev. C* **99**, 064615 (2019).
- [49] N. Hasegawa, K. Hagino, and Y. Tanimura, “Time-

- dependent generator coordinate method for many-particle tunneling,” *Phys. Lett. B* **808**, 135693 (2020).
- [50] P. Marević, D. Regnier, and D. Lacroix, “Quantum fluctuations induce collective multiphonons in finite fermi liquids,” *Phys. Rev. C* **108**, 014620 (2023).
- [51] P. Marević, D. Regnier, and D. Lacroix, “Multiconfigurational time-dependent density functional theory for atomic nuclei: technical and numerical aspects,” *Eur. Phys. A* **60**, 10 (2024).
- [52] B. Li, D. Vretenar, T. Nikšić, P. W. Zhao, and J. Meng, “Generalized time-dependent generator coordinate method for small- and large-amplitude collective motion,” *Phys. Rev. C* **108**, 014321 (2023).
- [53] B. Li, D. Vretenar, T. Nikšić, J. Zhao, P. W. Zhao, and J. Meng, “Generalized time-dependent generator coordinate method for induced fission dynamics,” *Front. Phys.* **19**, 44201 (2024).